Mesoscale Air Motions Associated with a Tropical Squall Line

JOHN F. GAMACHE AND ROBERT A. HOUZE, JR.

Department of Atmospheric Sciences, University of Washington, Seattle 98195

(Manuscript received 10 July 1981, in final form 7 December 1981)

ABSTRACT

Composites of radar and wind observations in a coordinate system attached to a moving tropical squall line confirm that such a squall system is composed of two separate circulation features: a convective squall-line region and a stratiform anvil region. The squall-line region is characterized by mesoscale boundary-layer convergence, which feeds deep convective updrafts, and mid-to-upper-level divergence associated with outflow from the cells. The anvil region is characterized by mid-level convergence, which feeds both a mesoscale downdraft below the anvil and a mesoscale updraft within the anvil cloud. Before this study, the mesoscale updraft in the anvil cloud of the tropical squall system had been somewhat speculative, and both the anvil updraft and downdraft had been inferred only qualitatively. The occurrence of the anvil updraft is now proven and quantitative profiles of the mesoscale anvil updraft and downdraft have been obtained.

1. Introduction

The tropical "squall line" (or "disturbance line") was first described as a distinct meteorological phenomenon by Hamilton and Archbold (1945). The first documentation of a tropical squall line observed during an organized field experiment was presented by Zipser (1969). Later field experiments have shown further details of these systems (Betts *et al.*, 1976; Zipser, 1977; Houze, 1977; Fortune, 1980). Knowledge accumulated from these studies has been reviewed by Houze and Betts (1981).

The tropical squall line is part of a propagating mesoscale disturbance, which we shall refer to as the "squall system". The squall line is the leading portion of the squall system and consists of cumulonimbus cloud elements. An extensive precipitating "anvil cloud" (as defined by Brown, 1979) trails the squall line.

The convective elements comprising the squall line are examples of "hot towers" of the type discussed by Riehl and Malkus (1958) and Riehl and Simpson (1979). They contain buoyant updrafts that carry air of high moist static energy from the boundary layer to the upper troposphere. Negatively buoyant downdrafts associated with the towers carry air of low moist static energy downward from the low to middle troposphere into the boundary layer. A portion of this convective downdraft air spreads forward and produces the squall (or gust) front at the leading edge of the mesoscale system, while another portion spreads to the rear of the system.

The anvil region, in contrast to the highly convective squall line, has a predominantly stratiform structure. The cloud and precipitation in this region tend to be horizontally uniform, with distinct vertical layering. Precipitation particles in the upper portions of the anvil cloud are in the form of ice particles, which, as they drift downward, grow by deposition, riming and aggregation, melt in a shallow layer, and finally evaporate partially as they fall to the surface through unsaturated air below the base of the anvil. The layer in which the particles melt appears on radar as an extensive bright band of the type normally associated with stratiform precipitation. Leary and Houze (1979b) have described the stratiform precipitation structure in the anvil region, including the melting band, and have estimated the cooling rates associated with both the melting and the evaporation. The stratiform nature of the precipitation in the anvil region indicates that the vertical air motions throughout this region must be weak, that is, small compared to the fallspeeds of the precipitation particles (Houze, 1981).

The vertical motions in the anvil region are downward below the base of the anvil and appear to be upward within the anvil cloud itself (Fig. 1). The existence of the mesoscale subsidence below the anvil is generally accepted. It is shown by the penetration of low moist static energy to low levels throughout the anvil region (Zipser, 1969). From observed horizontal divergence, Zipser (1977) calculated the mesoscale downdraft vertical velocity to be 10 cm s^{-1} at a level near the top of the boundary layer. Mesoscale downdraft motion of similar magnitude occurred below the anvil of a tropical squall system simulated numerically by Brown (1979).

The existence of the mesoscale updraft in the anvil

0027-0644/82/020118-18$08.50

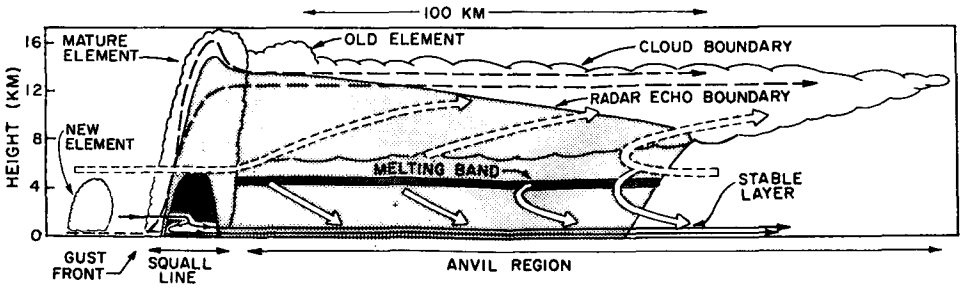

FIG. 1. Schematic cross section through squall system. Associated with the mature squall-line elements, dashed streamlines show convective-scale updraft, solid streamlines show downdraft circulation. Associated with the trailing anvil, wide solid arrows show mesoscale downdraft circulation, wide dashed arrows show mesoscale updraft circulation. Dark shading shows strong radar echo in the melting band and in the heavy precipitation zone of the mature squall-line element. Light shading shows weaker radar echoes. Scalloped line indicates visible cloud boundary.

cloud has not been established as convincingly as the mesoscale downdraft. However, it is strongly suggested by a variety of evidence. For example, Leary and Houze (1980) diagnosed an anvil updraft of peak magnitude 40 cm s^{-1} from the thermal stratification and horizontal winds in the anvil region of a tropical squall system. A mesoscale updraft occurred in the anvil cloud of Brown's (1979) model. Mid-latitude squall lines similar to tropical squall lines exhibit mesoscale anvil updrafts (Sanders and Paine, 1975; Sanders and Emanuel, 1977; Ogura and Chen, 1977; Ogura and Liou, 1980). Finally, the net vertical motion over large-scale regions partially occupied by tropical squall systems has been found to be upward in the mid to upper troposphere (Frank, 1978; Ogura *et al.*, 1979).

Although the occurrence of the anvil downdraft in tropical squall systems is accepted and the updraft is suggested strongly by studies cited above, the indications of these features from data have been primarily indirect and qualitative. It has been difficult to determine the vertical distributions of vertical velocities in anvil regions because of the sparsity of wind observations, even in special field experiments. In this paper, we present such profiles for the first time. Surface and upper-air wind observations are composited with respect to the radar echo pattern of a tropical squall line. Frank (1978) and Tourre (1979) have composited wind data with respect to satellite imagery of tropical squall lines. However, these satellite composites do not distinguish the anvil portion of a squall system from its line of convective cells. The ability of the radar to identify the horizontally uniform precipitation falling from the anvil and distinguish it from the intense vertical cells that characterize the squall line makes it possible for us to locate wind observations with respect to the squall line and anvil regions separately. From the wind pattern in the radar-delineated anvil area, the vertical profiles of divergence within and below the anvil cloud can be obtained, and, from these profiles, the vertical velocities in the mesoscale anvil updrafts and downdrafts can be determined.

In this study, we use the technique of compositing wind observations in relation to radar echo patterns for the tropical squall line that passed over the ship network of the Global Atmospheric Research Programme's Atlantic Tropical Experiment (GATE) on 12 September 1974. This squall line and various aspects of its structure have been described by Houze (1975), Shupiatsky *et al.* (1976), Mandics and Hall (1976), Zipser (1977), Nitta (1977), Mansfield (1977), Gaynor and Mandics (1978) and Leary and Houze (1979b).

2. Data

a. Radar data

Eight of the ships in the GATE observational network carried weather radars (Arkell and Hudlow, 1977). Four of the radars were C-band (5 cm wavelength) and equipped for digital data acquisition. Details of the characteristics and accuracy of the four C-band systems are given by Hudlow *et al.* (1980). Brief summaries of various aspects of the GATE C-band radar data can also be found in Houze (1977), Houze and Cheng (1977), Leary (1978), Cheng and Houze (1979) and Hudlow (1979). The GATE radar data are available on film and magnetic tape through the GATE Data Catalog.[1]

In this study, we have used data from C-band radars aboard the ships *Researcher, Oceanographer* and *Quadra*. On the day of our case study, the *Oceanographer* radar's antenna platform was not properly stabilized, and its data were of limited use. The primary data were from the *Researcher*.[2]

[1] Available from National Climatic Center, Asheville, NC 28801.

[2] Prof. Houze was the radar scientist aboard the *Researcher* during the passage of the 12 September 1974 squall line.

b. Wind data

Surface winds used in this study were obtained from Dr. K. Ooyama.[3] These winds were band-pass filtered to eliminate high-frequency fluctuations. Mesoscale features (~100 km in horizontal dimension), however, were not removed, and the winds form a coherent pattern in the region of the squall system.

Upper-air wind observations were obtained for the 15 ships in the GATE A/B and B arrays. The final validated data were used. At the 900, 850 and 450 mb levels, the ship data were supplemented by wind measurements obtained aboard the NOAA C-130 aircraft. Aircraft wind data were also obtained from the NCAR L-188 (Electra) aircraft at 960 mb and from the NASA CV-990 aircraft at 200 mb. Both the ship and aircraft upper-air data are available through the GATE Data Catalog (see footnote 1).

3. Construction of the composite squall system

To construct a composite squall system, all wind data obtained between 0900 and 1800 GMT were plotted in a common coordinate system attached to the traveling squall line. In this section, we describe how the common coordinate system is located with respect to the squall line and how data are transferred from geographical coordinates to the common coordinate system.

First, the squall line was located by plotting the leading edge of the rapidly moving radar echo associated with the squall system. As in the schematic (Fig. 1), the intense convective-scale precipitation elements associated with the squall line occurred just behind the leading edge of echo. Isochrones of the leading edge of the squall-line echo are shown in Fig. 2. The line progressed southwestward at an average speed of 13.5 m s^{-1}. Large irregularities occasionally occurred in the shape of the line from one hour to the next. The most extreme change in shape occurred between 1200 and 1300 GMT. These changes were the result of discrete squall-line propagation (Houze, 1977). Discrete propagation occurred when a squall-line element occasionally formed ahead of the line, and, as it strengthened, a new squall front became established at its leading edge, while old line elements to its rear weakened and blended into the trailing stratiform anvil region. This discrete component of propagation was combined with a continuous translational component to give the net squall-line motion shown by the isochrones.

To locate the common coordinate system with respect to the moving squall line, a point was chosen for each hour to represent the origin of the common system. This point was taken to be the squall-line center, defined as the point that most nearly satisfied all of the following simultaneously: (i) the forward-most point on the squall line, (ii) the point that bisected the portion of the squall line detected by radar, and (iii) the point providing the smoothest motion from hour to hour.

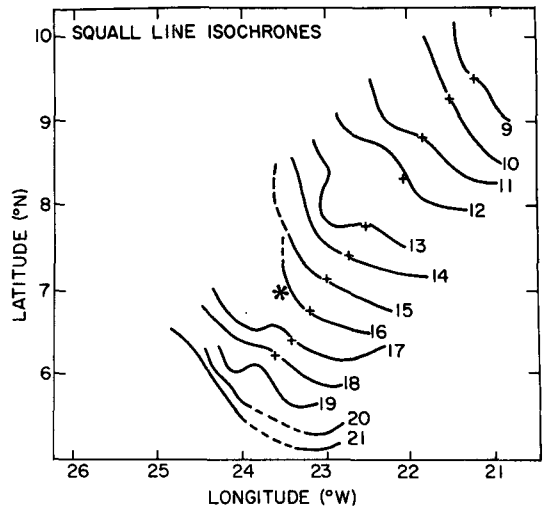

FIG. 2. Isochrones of leading edge of squall-line echo. Crosses indicate location of squall-line center for each hour. Dashed lines indicate the assumed location of squall line in regions between squall-line echoes. Asterisk indicates location of the ship *Researcher*.

The squall line centers are shown in Fig. 2 as crosses. The position of the center between hours was obtained by linear interpolation.

Data were transferred from geographic to common coordinates by positioning the origin of the common (α, β) coordinate system over the squall-line center, with the α-axis pointing 37° east of true north (Fig. 3). The β-axis was oriented perpendicularly to the α-axis. Composite patterns were obtained by trans-

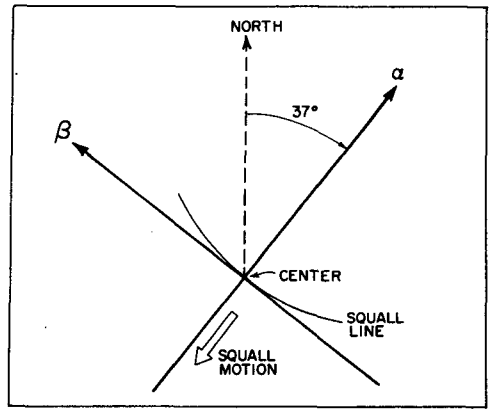

FIG. 3. Coordinate rotation for composite coordinate system. Curved line indicates idealized shape and orientation of squall-line which moves in the negative α direction. The α-axis is located 53° counterclockwise from the x (west–east) axis and the β-axis is located 53° counterclockwise from the y (north–south) axis.

[3] Present affiliation: National Hurricane Research Laboratory, Coral Gables, FL 33146

ferring data for a series of map times into the α-β plane, each time locating the origin of the α-β plane at the current squall-line center. This procedure assumes the squall system was in an approximately steady state throughout the period covered by the series of map times. Although the pattern of convective-scale elements within the squall line was undergoing fluctuations during this time, the mean features of the line and anvil region, on a horizontal scale of ~100 km, were indicated by radar to be quasi-steady throughout a period from 0900–1800 GMT on 12 September, though the later hours were beginning to show signs of dissipation. We used wind data from this entire time period, and radar data from 1300–1800 GMT (the period during which the line was within range of the *Researcher* radar), and our composite may be considered to be of the mature to early dissipating stage of the squall system.

4. Composite radar echo pattern

By transferring radar observations to α-β coordinates, a composite radar-echo pattern was obtained for the squall system. First, echo patterns at each hour, on the hour, from 1300 to 1800 GMT were analyzed to identify the squall-line (S) and post-squall anvil (A) regions. The boundaries of the S and A regions for each hour were transferred to the common coordinate system as described in Section 3. The squall-line composite echo (Fig. 4a) is the region of the α-β plane into which all the individual S regions fell (i.e., it is the union of all the S regions for individual hours). The anvil composite echo (Fig. 4b) is the region of the α-β plane into which all the individual A regions fell. Subregions of the squall-line and anvil echoes, within which precipitation was observed 3–4 h and 5–6 h out of the 6 h included in the radar composite, are shown by shading. The shading does not indicate the location of the maximum radar reflectivity through the 6 h period, but instead it represents the location of the most frequently observed echo. The most frequently observed echo in the S region occurred in the left half of the squall line; however, the stronger echoes were in the right half. The position of the left half of the squall line varied little while the right half exhibited more discontinuous motion so that the area in which the convective-scale echo might have been seen was greater. The average thickness of the squall-line echo for any individual observation was ~20 km.

Prior to transferring their boundaries to the common coordinate system, the S and A regions were identified at each individual hour by taking into account echo intensity, horizontal gradient of reflectivity, steadiness or unsteadiness of echo patterns, presence or absence of vertical echo cores, and presence or absence of a radar bright band. In general, the S region was characterized by rapidly fluctuating

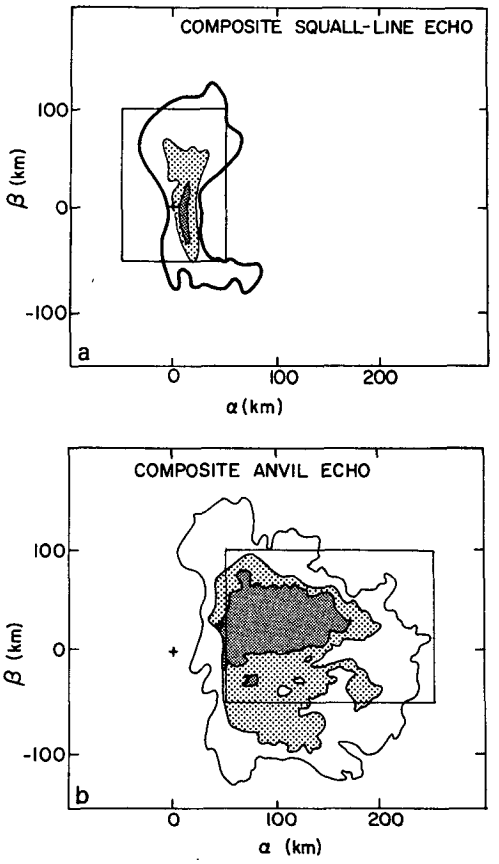

FIG. 4. Composite radar echoes for (a) the squall-line (or convective echo) region and (b) the anvil (or stratiform echo) region. Irregular outer boundaries in (a) and (b) enclose the area within which echo was seen at some time during the composite period. Boxes indicate regions for which average divergences were calculated for the squall-line (a) and for the anvil region (b). Shading indicates the frequency that anvil echo was seen, the interior region covering the region within which squall-line (a) or anvil (b) echo was observed 5–6 out of 6 h, the intermediate region 3–4 out of 6 h and the outer region 1–2 out of 6 h.

intense echoes [$\geq$38 dB(Z) or 14 mm h^{-1} in rainfall rate] in vertically oriented, but tilted, cores bounded by strong horizontal gradients of reflectivity. The A region, in contrast, exhibited generally weaker echo [$\leq$38 dB(Z)], which tended to be horizontally uniform [reflectivity gradients generally $\leq$1 dB(Z) km^{-1}], and characterized by a bright band. The leading edge of the S region was given by the leading edge of echo shown by isochrones in Fig. 2. The back edge of the S region (or front edge of the A region) was located by subjective judgement based on all the descriptive characteristics listed above. Not all the characteristics could be identified at any given hour. For example, when the squall line was far from the radar, the vertical resolution of the observations was insufficient to determine the presence or absence of a bright band. However, as many as possible of the observed characteristics were sought to identify the S and A regions at a given time. In general, the back

edge of the S region was found where the echo intensity dropped to <38 dB(Z) and the horizontal reflectivity gradient dropped to ≤1 dB(Z) km^{-1}. The S region contained all echo enclosed by the front and back edges and the ends of the squall line (as seen on radar). The A region consisted of all echo within the squall system but located to the rear of the back edge of the S region.

Fluctuations in the boundary between the S and A regions from one map time to the next occasionally led to the back portion of S at one map time occupying the same α-β coordinates as the leading portions of A at other times, with the result that there are small areas of overlap between the anvil composite echo and the squall-line composite echo (compare Figs. 4a and 4b).

The boxes in Fig. 4 outline regions for which divergence is computed from the composite wind patterns discussed in subsequent sections. The smaller box is hereafter referred to as the squall-line region while the larger box is referred to as the anvil region.

5. Composite wind patterns

Observed winds were composited in α-β coordinates in the manner described in Section 3. From the analysis of the observed winds, values for wind velocities on a 50 km × 50 km horizontal grid were determined. The grid values of velocity were then used to generate relative wind composites that were consistent with the observed winds. By relative winds, we mean the observed winds minus the average velocity of the squall line (13.5 m s^{-1} from 37°). Divergence was also calculated on a 50 km × 50 km grid using the grid values from the analysis of observed velocity. The composite patterns have been constructed for the surface, 960, 900, 850, 650, 450, 300 and 200 mb levels. Plotted winds, streamline and isotach analyses, and patterns of divergence are shown in Figs. 5–10 for all levels except 960 and 900 mb. The maps of divergence are based on the computed grid values of divergence. They do not include the correction, applied later, to compute vertical velocities (Section 6a).

a. Surface winds

Three major mesoscale features can be seen in the surface composite wind field (Fig. 5). First, a line of confluence is seen ahead of the squall-line region. The line is most evident in the observed winds (Fig. 5a), and it is associated with a region of maximum convergence with values 10^{-4} s^{-1} in magnitude (Fig. 5c). This confluence line coincided with a line of convection that intersected the squall line at right angles (see Fig. 3b of Shupiatsky *et al.* 1976).

The second major feature of the surface composite winds seen in Fig. 5 is the squall line itself, centered,

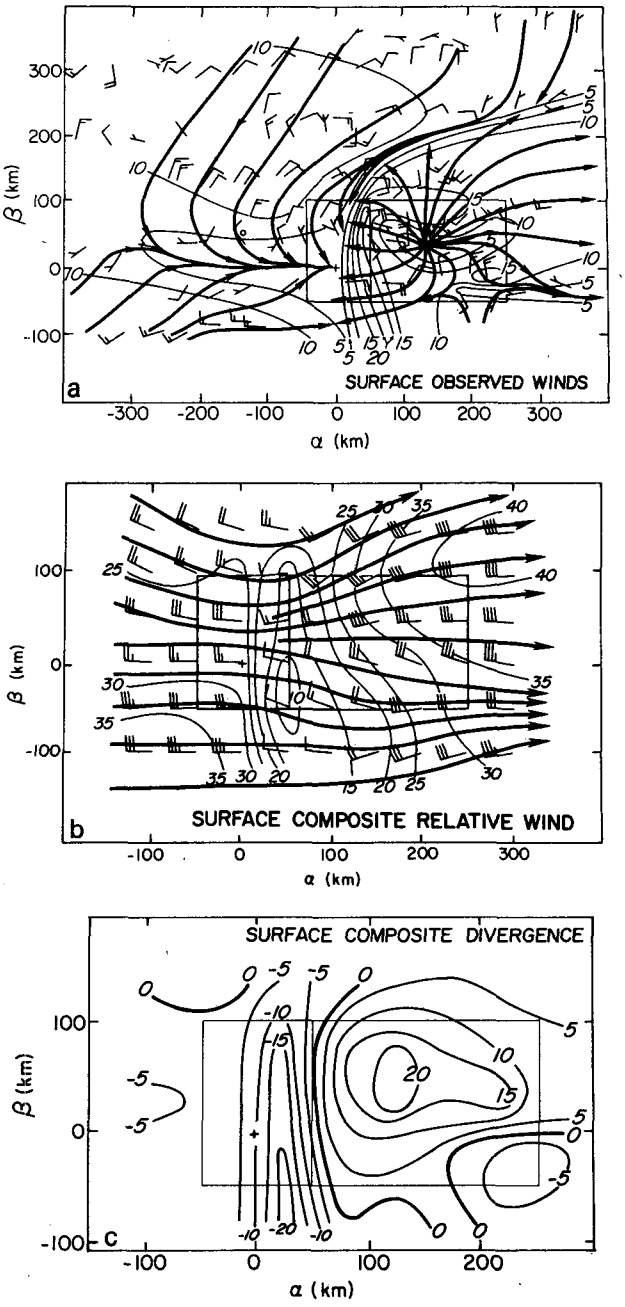

FIG. 5. Composite observed surface winds with (a) streamline and isotach analysis. Cross indicates squall-line center and origin of the α-β coordinate system. Solid contours indicate wind speed in knots. Full wind barb is for 10 kt (or 5 ms^{-1}) and half barb is for 5 kt (or 2.5 m s^{-1}). Box to the left is the squall-line region as in Fig. 4a and box to the right is the anvil region as in 4b. (b) Composite of surface relative winds, streamlines and isotachs as in Fig. 5a. (c) Divergence pattern for surface composite wind in units of 10^{-5} s^{-1}.

as expected, on the origin of the composite. The squall line is evident as a zone of convergence enclosed by the box denoting the squall-line region. The third major feature is the nearly pure divergence

pattern seen in the surface flow in the anvil region [compare Fig. 17-6 of Haltiner and Martin (1957) with our Fig. 5a]. Some anticyclonic curvature of the divergent streamlines is also evident. This divergent outflow is centered on the central core of the anvil composite echo (cf. Fig. 4b). This result is expected; the divergence is apparently associated with evaporative cooling and subsidence below the precipitating anvil cloud. However, the result is not automatic since the radar and wind patterns are composites of independent sets of data.

The convergence in the squall-line region is accounted for by weak observed flow ahead of the line and strong flow into the rear of the squall-line region from the divergent anvil region (Fig. 5a). In relative flow, the wind throughout the region ahead of the line is directly into the squall line region at speeds of 12–15 m s^{-1} but comes to a near halt in the squall region (Fig. 5b). The narrow region of reversed relative wind behind the squall line cannot actually be resolved by the data plotted in Fig. 5; however, its existence is evident from the continuous surface wind traces at individual ships over which the line passed (Fig. 11). The relative wind normal to the squall line suddenly dropped below zero at squall-line passage, then gradually increased for the next several hours at each ship. This steady increase after squall passage is evident also in Fig. 5b; from the back of the squall region to the back of the anvil region, there is a relative flow out of the region, which increases in strength toward the rear of the system.

The relative wind flow in Fig. 5b conforms quite well to the pattern seen in other tropical squall-line systems, where pre-squall boundary-layer air is stripped from the surface (in the region of reversed-relative wind) and replaced in the post-squall region by a wake of downdraft air (Fig. 1).

b. 850 mb winds

The most striking feature of the 850 mb wind composite is the jet in the observed wind field through the left[4] portion of the anvil region (Fig. 6a). This jet increased in speed in the middle of the anvil region, slowed in the left forward part, and came to a halt in the squall-line region. The relative winds in Fig. 6b show that the 850 mb air was entering the squall-line region strongly from the front and more weakly from the left end and left rear of the line. This change in direction of the relative flow across the left portion of the line indicates that, on entering the squall-line region, the 850 mb air traveled either upward or downward rather than through the squall line.

The relative inflow all along the front of the squall system (Fig. 6b) was the result of the observed winds being parallel to the propagating line (Fig. 6a). Relative flow at the rear of the anvil region was out the back. Relative inflow at the front of the squall-line region and outflow at the rear of the anvil region is typical of the 850 mb flow in tropical squall systems (Zipser, 1969, 1977; Betts *et al.* 1976; Houze, 1977).

The pattern of divergence in the anvil region was complex at 850 mb. Winds were convergent in the

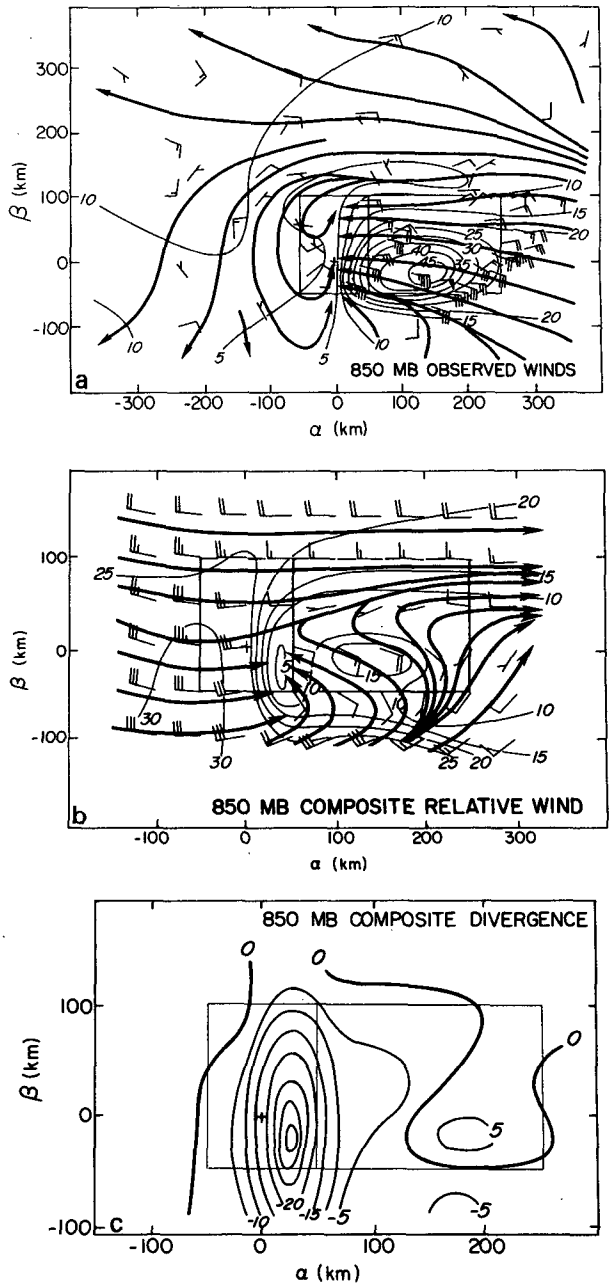

FIG. 6. Streamline and isotach analysis of 850 mb observed winds (a), 850 mb relative winds (b), and 850 mb divergence analysis (c). Otherwise, As in Fig. 5.

[4] We will use "left" and "right" to refer to lower and higher values, respectively, of the coordinate β.

front of the region, divergent in the left rear, and basically non-divergent in the right rear of the region (Fig. 6c).

c. 650 mb winds

At the 650 mb level, the observed flow (Fig. 7a) over most of the right portion of the composite region was 15–20 m s^{-1} and generally parallel to the α-axis. This feature was the jet ahead of the trough of an African easterly wave (Reed *et al.*, 1977). A zone of strong cyclonic shear, separating the jet from weaker flow throughout the forward left portion of the composite region, lay across the right portion of the squall system. In the relative flow pattern, the cyclonic shear of the observed flow became a cyclonic vortex concentrated in the rear half of the region. Evidence of cyclonic vorticity at the 600–700 mb level has been noted in the mature to late stages of development of other tropical squall systems (Fig. 5c of Houze, 1977; Fig. 12b of Fortune, 1980) and in the anvil region of a non-squall tropical cloud system (Fig. 2 of Leary, 1979).

The relative flow pattern at 650 mb in our case shows flow into the squall-line region from the front. This flow continues through the squall-line region into the anvil region. Flow also entered the anvil region from the rear. This pattern is consistent with previous studies of tropical squall lines, which typically show weak relative inflow from both front and back (Fig. 5 of Obasi, 1974; Fig. 5 of Betts *et al.*, 1976; Fig. 7 of Houze, 1977). Our own Fig. 7b shows the inflows from front and rear meeting in the center of cyclonic rotation in the anvil region. Inflow and outflow also occurred along the left and right sides of the anvil region, in association with the rotation. Within the anvil region, convergence was dominant as can be seen in Fig. 7c. Convergence at the base of the anvil is important in indicating, as will be shown in Section 6c, that 650 mb is a level lying between a mesoscale updraft above and a mesoscale downdraft below.

d. 450 mb winds

The major features of the observed wind at 450 mb (Fig. 8a) were diffluence over the squall-line region and the surface confluence line ahead of the squall line, and confluence at the rear of the anvil region. The relative flow (Fig. 8b) was through the squall system with rather uniform direction and speed convergence at the rear of the anvil region. Calculations of divergence show that convergence occurred in this region (Fig. 8c). Weak divergence was found over the squall-line region and over the confluence line normal to the squall line, where diffluence was evident in the observed winds.

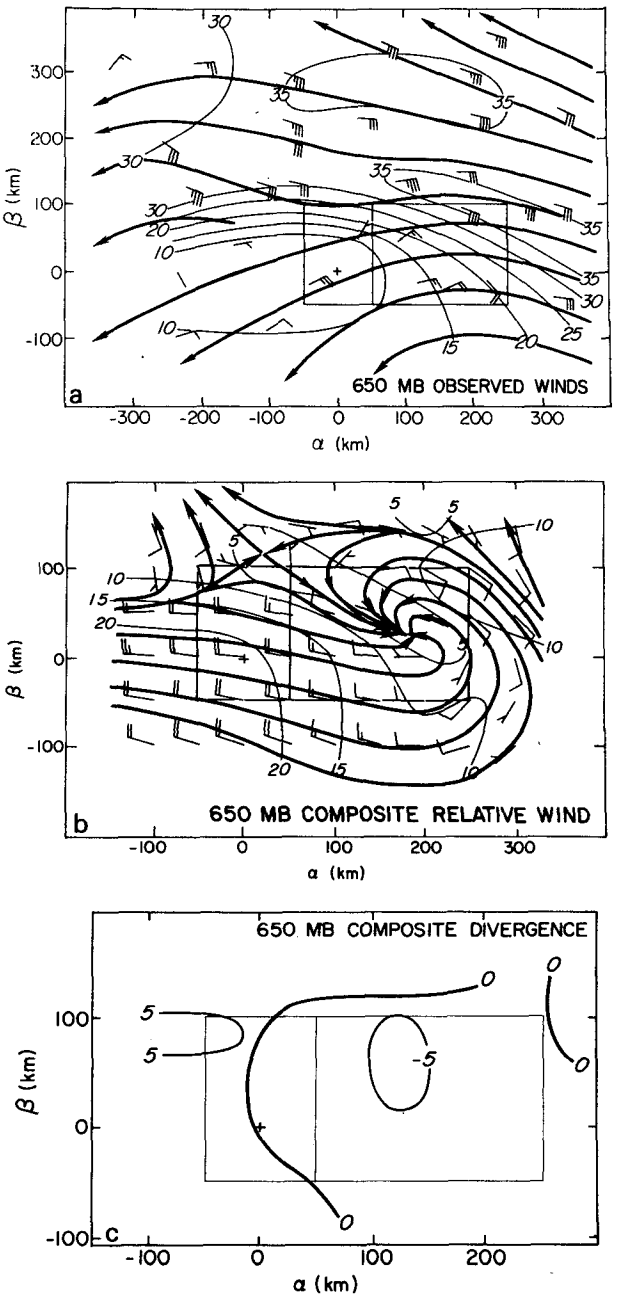

FIG. 7. As in Fig. 6, for 650 mb.

e. 300 mb winds

At 300 mb, the flow in both the observed and relative winds (Figs. 9a and 9b) was mildly diffluent over the right portions of the squall-line region and over the region ahead of the squall-line occupied by the line of surface confluence. Calculations show nearly non-divergent conditions in the anvil region as a whole and divergent conditions in the squall-line and pre-squall regions (Fig. 9c). The relative flow

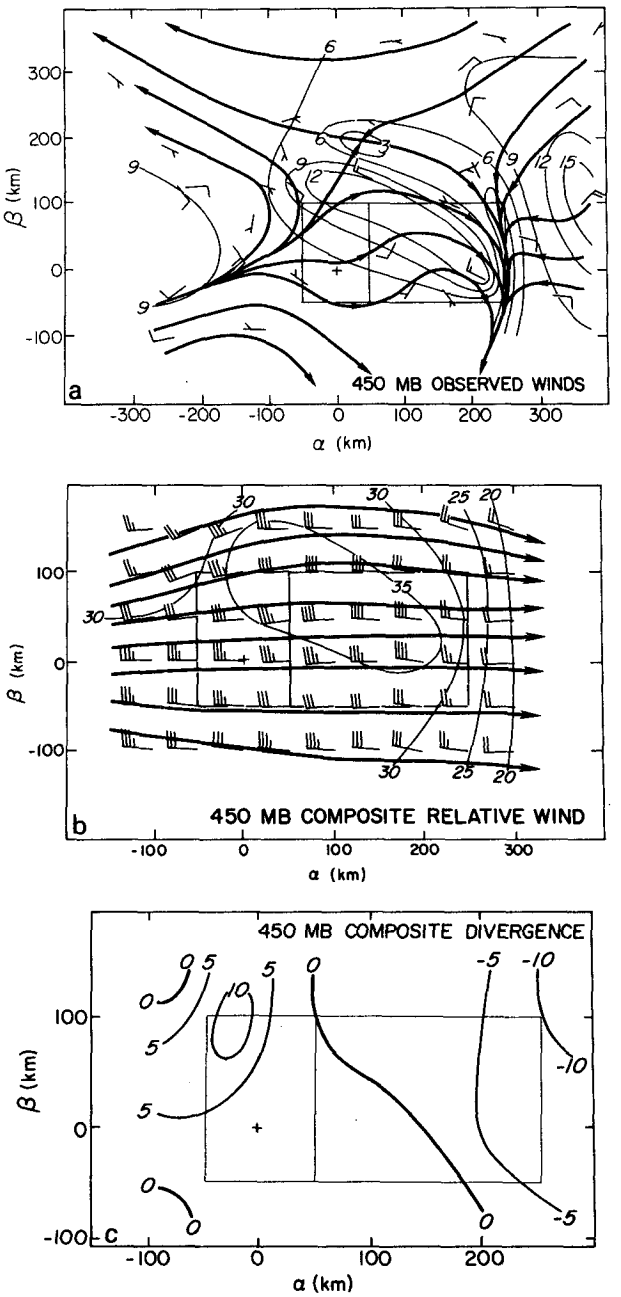

FIG. 8. As in Fig. 6, for 450 mb.

was through the squall-line system, directly from front to rear at 12–15 m s^{-1}, in a pattern resembling that at 450 mb (compare Figs. 8b and 9b).

f. 200 mb winds

In the observed winds at 200 mb (Fig. 10a), a diffluent anticyclonic streamline pattern was evident throughout the composited area. Relative winds flowed through the squall-line and anvil regions, generally from left front to right rear (Fig. 10b). The diffluence seen in the winds was especially apparent in the anvil region, where the direction of the wind into the left border of the box changed by ~60° between the front and back ends of the box. This diffluence was the primary factor contributing to an average divergence of 5×10^{-5} s^{-1} in the anvil region (Fig. 10c). The divergence was strongest in the left-rear portion of the region. Diffluent winds at 200–

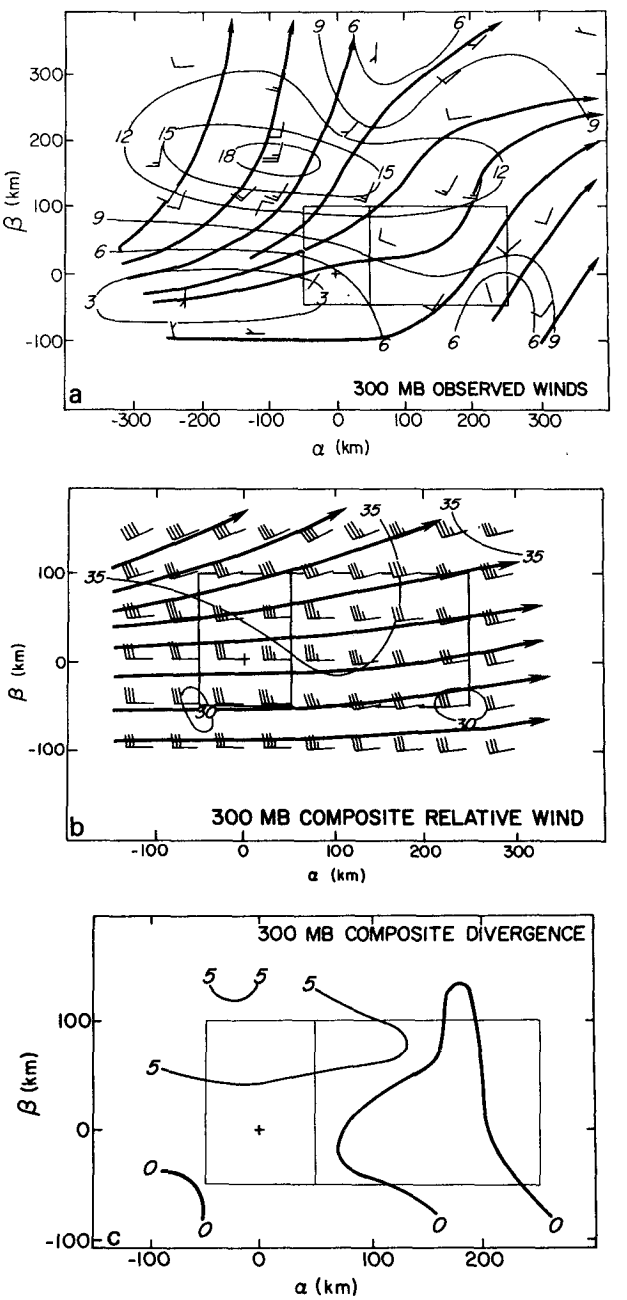

FIG. 9. As in Fig. 6, for 300 mb.

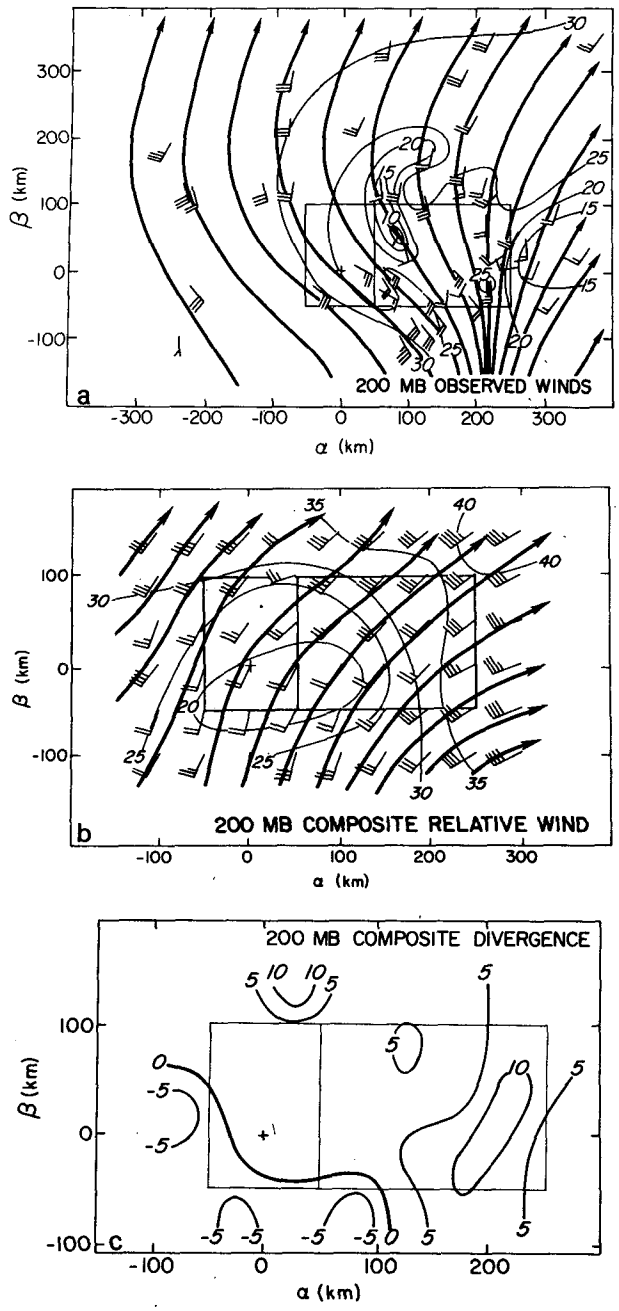

FIG. 10. As in Fig. 6, for 200 mb.

250 mb have been noted in the mature to late stages of development of other tropical squall systems (Fig. 5c of Houze, 1977; Fig. 13a of Fortune, 1980), in the anvil region of a non-squall system (Fig. 3b of Suchman and Martin, 1976; Fig. 2 of Leary, 1979), and in association with mid-latitude convective complexes (Maddox, 1980; Fritsch and Maddox, 1981a). Maddox (1980) showed that the diffluent upper-level flow was a superposition of a relatively uniform synoptic-scale flow and a mesoscale center of divergence and anticyclonic rotation. In this study, the observed synoptic-scale wind appears, rather similarly, to be a diffluent flow from left to right with some anticyclonic turning. The squall-line system appears to be a superimposed divergent region of outflow.

The spot of weak winds seen near the right front corner of the anvil region in Fig. 10a is somewhat of a mystery. It is tempting to explain this feature as a region of air of low horizontal momentum extruded from the tops of convective updrafts since the spot of weak winds is downstream (in the relative winds shown in Fig. 10b) from the squall-line region, where deep convective cells were located. However, it could be argued that it is too far downwind.

6. Divergence and vertical air motion in the composite squall system

a. Method of computation

In this section, we describe horizontal divergence and vertical motion calculated from the composite wind maps. Computations have been performed for the squall-line and anvil regions, defined by the boxes in Figs. 4–10. Computations were also performed for individual 50 km × 50 km grid squares in the region of the α-β plane for which divergence patterns are shown in Figs. 5c–10c. To demonstrate our methodology, let A represent an area for which divergence is calculated (i.e., A could be the area of the squall-line region, the anvil region or a single 50 km × 50 km grid square). The divergence over this area was computed from a line integral of the observed wind component v_n normal to the boundary of A, that is,

$$D_0(p) = A^{-1} \oint v_n(p)dl, \tag{1}$$

where $D_0(p)$ is the divergence at pressure p computed from observations. $D_0(p)$ is calculated for pressure levels of 1014 mb (surface pressure, called p_s in subsequent discussion), 960, 900, 850, 650, 450, 300 and 200 mb, which correspond to the levels for which composite maps were constructed. A vertical profile of divergence was obtained by fitting an Nth order polynomial to the values obtained for $D_0(p)$. This polynomial is of the form

$$D(p) = \sum_{i=0}^{N} B_i p^i, \tag{2}$$

where each B_i is a constant. Following O'Brien (1970), we assume that the error in the divergence is a linear function of pressure. The corrected divergence $D_c(p)$ is then written as

$$D_c(p) = D(p) + \epsilon(p_s - p), \tag{3}$$

where ϵ is a constant. The vertical velocity $\omega(=dp/dt$, where t is time) is computed by assuming $\omega(p_s) = 0$ and integrating:

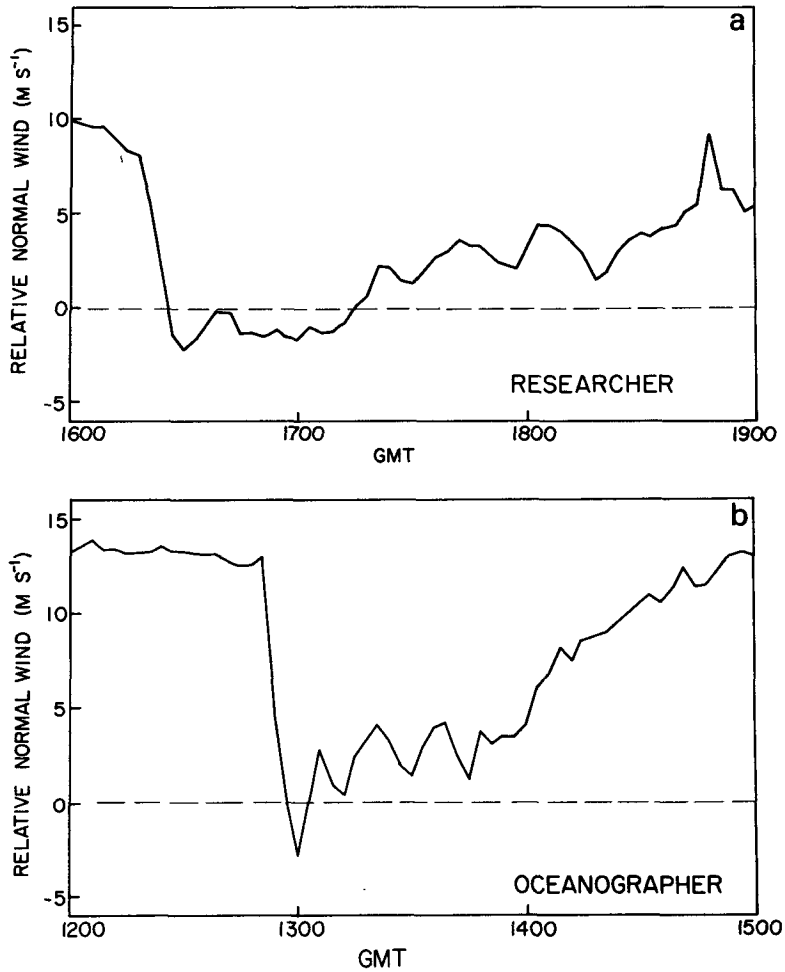

FIG. 11. Time series of surface relative wind component normal to the squall-line at the ships *Researcher* (a) and *Oceanographer* (b). Dashed line indicates zero relative speed.

$$\omega(p) = -\int_{p_s}^{p} D_c(p)dp$$

$$= -\int_{p_s}^{p} D(p)dp - \epsilon \int_{p_s}^{p} (p_s - p)dp$$

$$= -\int_{p_s}^{p} D(p)dp + \tfrac{1}{2}\epsilon(p_s - p)^2. \qquad (4)$$

Mass balance is achieved assuming that $\omega(p_T) = 0$, where p_T is the pressure at some high level. Then substitution of p_T in (4) yields a value for ϵ, given by

$$\epsilon = \frac{2\int_{p_s}^{p_T} D(p)dp}{(p_s - p_T)^2}. \qquad (5)$$

Substitution of this expression for ϵ in (3) and (4) gives the corrected divergence $D_c(p)$ and vertical velocity $\omega(p)$.

The calculated values of $\omega(p)$ at 100 mb for the squall-line region and at 150 mb for the anvil region were equal to 40% and 24% of the extreme values of ω throughout the tropopause. This required a correction of 3×10^{-5} s^{-1} at 100 mb for the squall-line region and 0.5×10^{-5} s^{-1} at 150 mb for the anvil region. As stated earlier these corrections decrease linearly to zero at the surface. Similar, but somewhat larger, corrections were needed for individual grid points.

The values of N, A and p_T used in our calculations of divergence and vertical motion are given in Table 1. For the squall-line and anvil regions, the divergences were calculated using a line integral of normal outflow around the border of each region. The corrected profile of divergence for each of the above regions is shown in Fig. 12 and the resulting vertical velocity is shown in Fig. 13. A similar line integral around each 50 km $\times$ 50 km square was used to compute grid point values of divergence. Analyses

TABLE 1. Values of N, A, and p_T used in divergence and vertical velocity calculations through Eqs. (1), (2), and (5).

Region for which divergence is calculated	N	A (km^2)	p_T (mb)
Squall-line region	3	1.5×10^4	100
Anvil region	4	3×10^4	150
Grid squares	3 for squall-line region, 4 for anvil region	2.5×10^3	100 for squall-line region, 150 for anvil region

of the uncorrected grid-point divergence values are shown in Figs. 5c, 6c, 7c, 8c, 9c and 10c. Grid point values were then corrected as shown in Table 1 in order to compute the vertical velocities shown in Figs. 15 and 16.

b. Divergence in the squall-line and anvil regions

The profiles of divergence $D_c(p)$ for the squall-line and anvil regions are shown in Fig. 12. In the squall-line region, convergence occurred in the lower troposphere, with the highest values between the surface and 850 mb. Soundings in the environment ahead of the squall-line show air of high moist static energy near the ocean surface, with lower energy air between 900 and 650 mb. Evidently, the strong convergence below 900 mb was feeding boundary-layer air of high moist static energy into the bases of convective updrafts, while the air converging between 900 and 650 mb was feeding convective downdrafts and being entrained into the sides of the convective updrafts (Fig. 1). Above the 650 mb level, the squall-line region was characterized by divergence, evidently associated with air detraining and spreading out from the upper portions of convective updrafts. The strongest divergence occurred near 200 mb, at the tops of the deepest cells. It is interesting that the divergence associated with cells was distributed fairly uniformly through a layer that corresponds precisely with the anvil cloud, whose base was near 650 mb. Evidently, divergent outflow from convective cells in the squall-line region was supplying material to the neighboring anvil cloud in a manner consistent with Fig. 1.

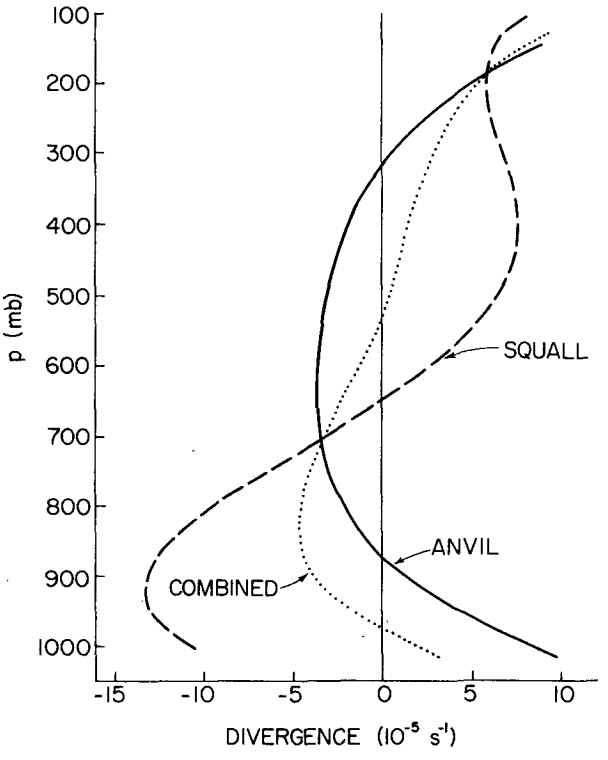

FIG. 12. Average divergence over the squall-line (dashed), anvil (solid) and combined (dotted) regions.

In the 700–650 mb layer, there is a state of nondivergence in the squall-line region (Fig. 12). This result is consistent with the conclusions of earlier studies (Zipser, 1969, 1977; Betts *et al.*, 1976; Houze, 1977) that the winds at this level tend to flow through the squall-line region (around and between the convective updraft towers) and into the anvil region (Fig. 1). Three-dimensional cloud models (e.g., Wilhelmson, 1974) also show the tendency for ambient air to flow around individual cumulonimbus towers at middle levels.

In the anvil region, convergence was located in middle levels, primarily beween 800 and 400 mb (Fig. 12). Strong divergence was found both above and below this layer. This divergence structure differs fundamentally from that of the squall-line region, where convergence was concentrated near the surface. Divergence profiles for the squall-line system as a whole (combining the squall-line and anvil regions) show an ambiguous combination or mixture of the two characteristic profiles of the squall-line and anvil regions. Only because the radar data allowed us to decompose the system into its two basic regions (Fig. 4) were we able to obtain the two distinct profiles.

Studies of winds in the vicinities of squall systems seen in satellite imagery (Frank, 1978; Ogura *et al.*, 1979) do not decompose the cloud system spatially into squall-line and anvil components. Satellite data of cloud tops cannot clearly distinguish the two regions. However, evidence of the characteristic squall-line and anvil profiles can be seen in the undecomposed wind data of the satellite studies if the life cycles of the squall systems are considered. Case-study analysis shows that squall systems and other major tropical cloud systems are primarily convective in their early stages, with anvil structures developing and taking on more importance in mid to late stages (Houze, 1977; Leary and Houze, 1979a; Houze *et al.*, 1981). Correspondingly, the undecomposed divergence profiles obtained by Frank (1978) and Ogura *et al.* (1979) for the early stages of squall

development resemble our profile for the squall-line region, while during later stages of system development, their profiles are more like an anvil-region profile.

c. *Vertical velocity and mass transport in the squall-line and anvil regions*

The vertical velocities in the squall-line and anvil regions, computed according to (4), are shown in Fig. 13. In the squall-line region, the vertical velocity increased with height to about 650 mb, where it was a maximum. The gradualness of the increase up to 650 mb can be explained by the existence of convective downdrafts, which would have increased in magnitude with decreasing height, reaching a maximum near cloud base. If such a convective downdraft vertical velocity were subtracted from the vertical velocity profile for the squall-line region shown in Fig. 13a, the resulting ω profile for updrafts alone would show a more constant value between cloud base and 650 mb, especially if the updraft entrainment rates were small.

To illustrate this conclusion, we have estimated the updraft and downdraft motions in the squall-line region. Simple parcel lifting exercises carried out on plotted pre-squall soundings (*Researcher* 1200, *Quadra* 0900 and *Oceanographer* 1200) indicate that parcels originating below 900 mb could not reach significant heights before becoming negatively buoyant. This air would be more likely to sink. We therefore assume that air converging below 900 mb rose on entering the squall-line region, while all the convergence between 900 and 650 mb in the squall-line region (Fig. 12) fed convective downdrafts. Accordingly, the estimated squall-line downdraft velocity (the dash-dot downdraft curve in Fig. 13b) increases from zero at 650 mb to a maximum at 900 mb. Below this level, the magnitude of the downdraft velocity is assumed to decrease linearly to zero. This decrease implies a divergence in the surface to 900 mb layer associated with spreading of the downdraft. The magnitude of convergence into squall-line updrafts in this layer is then the sum of the net squall-line convergence (Fig. 12) and this divergence of outflow. The dash-dot updraft curve (Fig. 13b) shows that the squall-line updraft velocity increases from zero at the surface to a maximum at 900 mb. Above 650 mb, divergence (Fig. 12) leads to a decrease of the updraft velocity. The decreasing magnitude of ω with height above 650 mb level in the squall-line seen in Fig. 13 again shows that outflow associated with convective cells was distributed throughout the mid to upper troposphere.

The fact that the maximum updraft velocity occurs at the 900 mb level in Fig. 13b seems low in view of in-cloud vertical velocity measurements such as those of LeMone and Zipser (1980) and general experience that a sounding ahead of a squall is not a good predictor of the squall line's convective properties unless it is lifted first. Cheng (1981) found it impossible to predict GATE convective cell heights realistically without first lifting the environment soundings. Following Cheng, we lifted the pre-squall sounding by the amounts indicated in Table 2. Using the lifted soundings, we found that parcels originating below 800 mb could reach significant heights. Therefore, the subdivision of the low-level convergence was redone assuming that all the convergence below 800 mb fed updrafts, while all the convergence above 800 mb fed convective downdrafts. Under this set of assumptions, the estimated squall-line downdraft velocity reaches a maximum at 800 mb and is lesser in magnitude than for the unlifted soundings, and the squall-line updraft velocity reaches its maximum at the 800 mb level (dotted curves in Fig. 13b), a somewhat more pleasing result in view of LeMone and Zipser's (1980) observations.

As pointed out in the Introduction and shown in Fig. 1, previous studies indicate both that a mesoscale downdraft occurs below the base of the anvil cloud and that a mesoscale updraft probably exists above the base of the anvil. Our vertical velocity profile for the anvil region in Fig. 13 shows that this was definitely the case in the GATE 12 September squall system. Zero vertical velocity occurred at 600 mb, near the usual base level of tropical anvil clouds. Upward motion occurred above this apparent anvil-base level, and downward motion occurred below. The composited wind and divergence patterns thus prove the vertical velocity structure long thought to exist in the anvil region. The vertical velocity w in height coordinates can be computed from ω by the hydrostatic approximation according to

$$w(p) \approx -\frac{\omega(p)}{\rho(p)g}, \tag{6}$$

where ρ is density and g the acceleration of gravity. Using the values of ω at the peaks of the anvil updraft and downdraft profiles in Fig. 13 (at p = 325 and 875 mb, respectively) and assuming ρ = 0.46 and 1.04 kg m^{-3} at p = 325 and 875 mb, respectively, we obtain w = 15 cm s^{-1} for the maximum of the anvil updraft and w = −6 cm s^{-1} at the level of the maximum anvil downdraft magnitude.

The mass of air transported vertically within area A during time τ is given by

$$M(p) = \rho(p)w(p)A\tau. \tag{7}$$

We let τ = 9 h, the length of time over which our composite applies, and substitute for w from (6). Then, the masses transported in the squall-line and anvil region may be expressed as

$$M_s(p) \approx -g^{-1}\omega_s(p)A_s\tau, \tag{8}$$

$$M_a(p) \approx -g^{-1}\omega_a(p)A_a\tau, \tag{9}$$

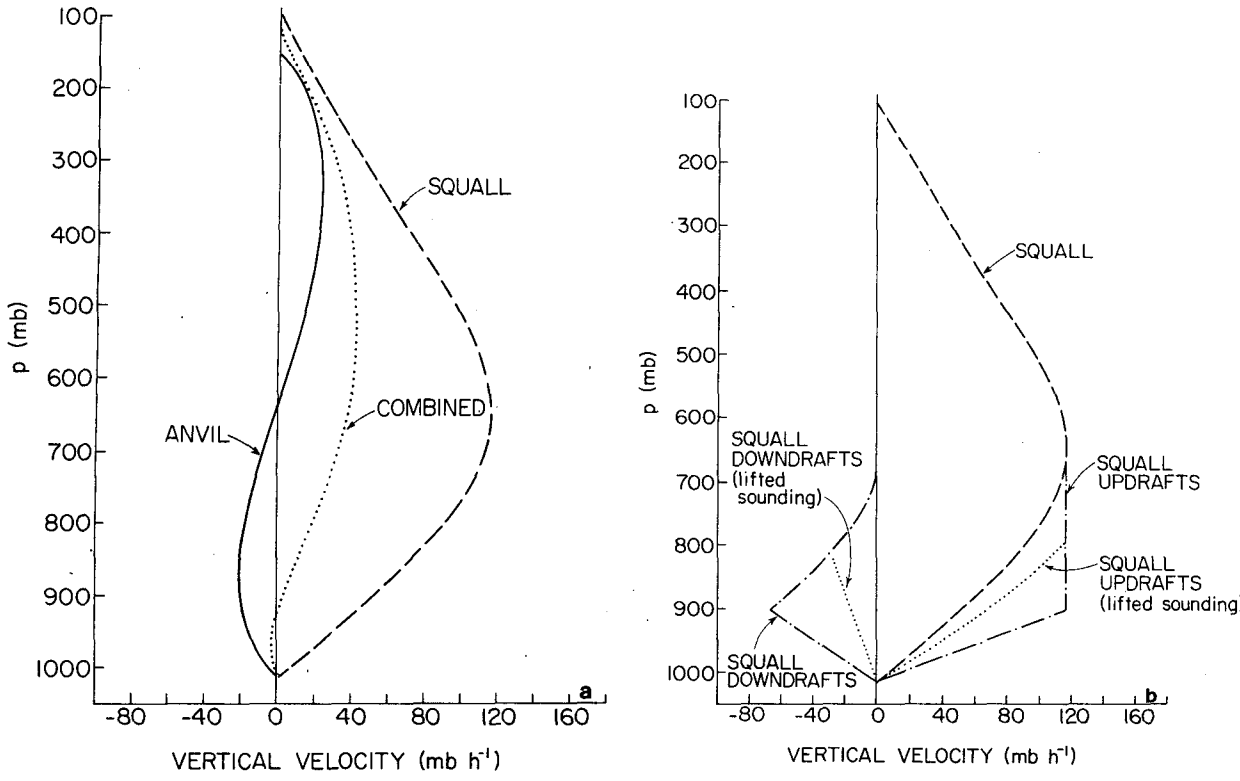

FIG. 13. Average vertical velocity (ω) for the squall-line (dashed), anvil (solid) and combined (dotted) regions (a), and for the squall-line updrafts and downdrafts in either lifted or unlifted pre-squall environments (b).

where subscripts s and a refer to the squall-line and anvil regions, respectively. The total mass transported vertically in the combined squall-line plus anvil region is

$$M_T(p) = M_s(p) + M_a(p) \tag{10}$$

and the average vertical velocity in the combined region is

$$\omega_T(p) = -\left(\frac{g}{A_T}\right) M_T(p). \tag{11}$$

The vertical velocity for the combined region (Fig. 13) shows the total upward air motion in the squall system to be concentrated aloft, with a small net downward motion at low levels. This combined vertical velocity structure has been found to be characteristic of the mid-to-late stages of tropical squall and non-squall cloud systems (Frank, 1978; Ogura, *et al.*, 1979) and of certain mid-latitude mesoscale convective systems (Ogura and Chen, 1977; Ogura and Liou, 1980; Fritsch and Maddox, 1981b). Our results of the tropical squall system and Ogura and Liou's results for a mid-latitude squall system show that the vertical profile for the total system is the natural result of combining the squall-line region's deep convective updrafts, which draw upon low-level convergence, with anvil vertical motions, which draw upon mid-level convergence.

The vertical transports of mass computed from (8)-(10) for the squall-line, anvil and combined regions are shown in Fig. 14. The combined-region profiles are similar to the total mass transport profile postulated by Leary and Houze (1980) to exist for an idealized squall system containing both an anvil updraft and an anvil downdraft (case C in their Fig. 8). This similarity lends support to their conclusions regarding the mass and heat transports by mesoscale system possessing anvil vertical motions.

d. Vertical cross sections of vertical motion

Cross sections showing vertical velocity in planes normal to the long axis of the squall-line box were determined by applying the method of computation of $\omega(p)$ described in Section 6a to the areas A covered by individual grid squares located at 50 km intervals along the lines defined by $\beta = -25$, 25 and 75 km in the composite coordinate system. The values of A, N and p_T used in computing $\omega(p)$ for each grid square are given in Table 1. The results are shown in Fig. 15.

The patterns of ω for each value of β are qualitatively similar. Each cross section shows a vertical

TABLE 2. Amounts by which pre-squall soundings were lifted.

Original pressure (mb)	Amount lifted (mb)	Original pressure (mb)	Amount lifted (mb)
1000	5.0	500	48.8
900	18.8	400	50.0
800	30.0	300	45.0
700	39.0	200	30.0
600	45.0	100	5.0

column filled with upward motion in the squall-line region. In the anvil region, downward motion was located in the lower troposphere, generally, with upward motion aloft. Ahead of the squall line, weak upward motion occurred in the lower troposphere while stronger downward motion existed aloft.

The squall-line vertical motion increased with decreasing β. The maximum ω increased from 130 mb h^{-1} at β = 75 km to 220 mb h^{-1} at β = −25 km. The maximum magnitudes of the anvil updraft and downdraft vertical motions were between 35 and 40 mb h^{-1}.

Figs. 15a and 15b show that the anvil updraft had a secondary maximum, which was not located directly above the anvil downdraft maximum, but was farther back, offset from the downdraft maximum by ~100 km. The anvil downdraft maximum coincided with the most frequent anvil rain, while the secondary upward updraft maximum was located near the rear of the anvil region, i.e. not directly over the rain area.

The offset of the anvil updraft and downdraft maxima was also found by Ogura and Liou (1980, see their Fig. 16) and in Brown's (1979) simulation of a tropical squall system (see his Fig. 11). In Brown's model simulation, the offset was related to the vertical shear of the horizontal wind normal to the squall line, and the amount of the offset increased with the age of the system. Since our composite squall system was in a mid-to-late stage of development, the large offset of the anvil updraft and downdraft should be expected, if the dynamics of the composite system are similar to Brown's model.

The strong downward motion aloft ahead of the squall line at α = −75 km is similar to the strong compensating motion in the immediate environment of convection discussed by Lilly (1960), Fritsch (1975), Sanders and Paine (1975), Hoxit *et al.* (1976), Fritsch and Chappell (1980) and Rosenthal (1980). This strong compensating motion might be expected in the mid-to-upper troposphere since this is the layer where the convective updrafts and the

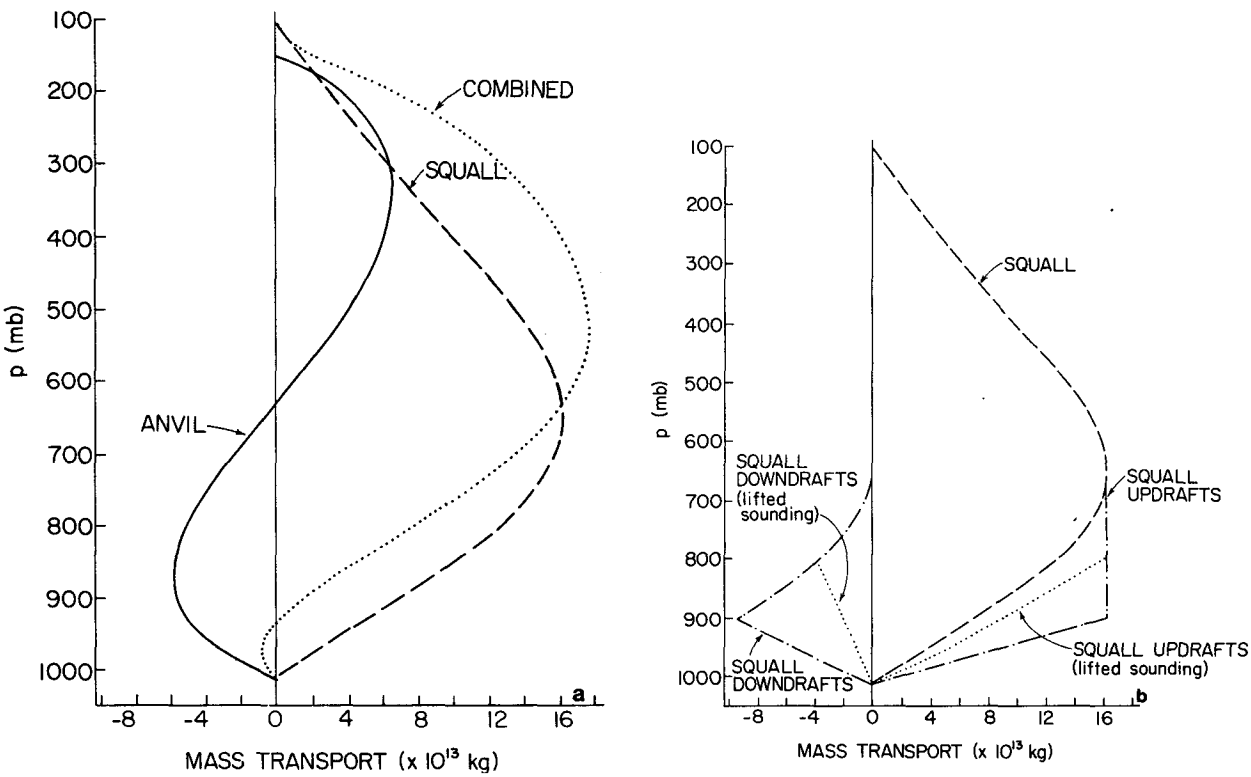

FIG. 14. As in Fig. 13 for the total mass transport (M) in each region.

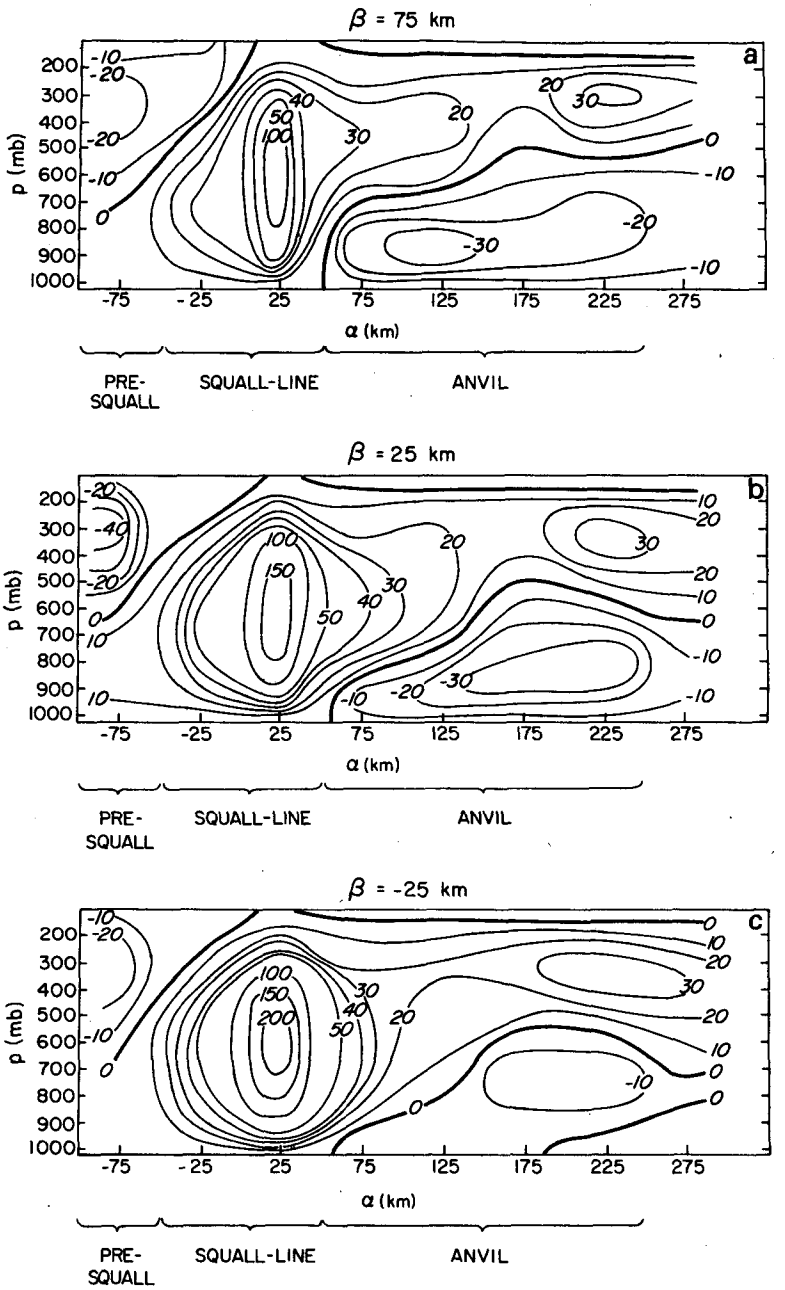

FIG. 15. Vertical velocity ω cross sections extending from front to back through the squall-line system along β = 75 km (a), β = 25 km (b) and β = −25 km (c). Contours are labeled in mb h^{-1}.

anvil updraft combine to produce a large upward motion which must be compensated. The compensating downward motion aloft ahead of the line may be involved in the squall line's propagation [see discussion of squall-line propagation in Houze and Betts (1981)]. The lack of environmental subsidence in the lower troposphere is expected since the upward motion of convective updrafts is nearly cancelled by convective and anvil downdrafts, so that less environmental compensating motion is necessary.

7. Two-dimensional airflow relative to the composite squall system

In Fig. 16, the component of the horizontal wind normal to the front of the squall-line region and vertical motions from Fig. 15 have been combined to construct the airflow relative to the squall system in the α-p plane, along the lines defined by β = −25, 25 and 75 km. The relative flow thus obtained is shown for the pre-squall region and the anvil region

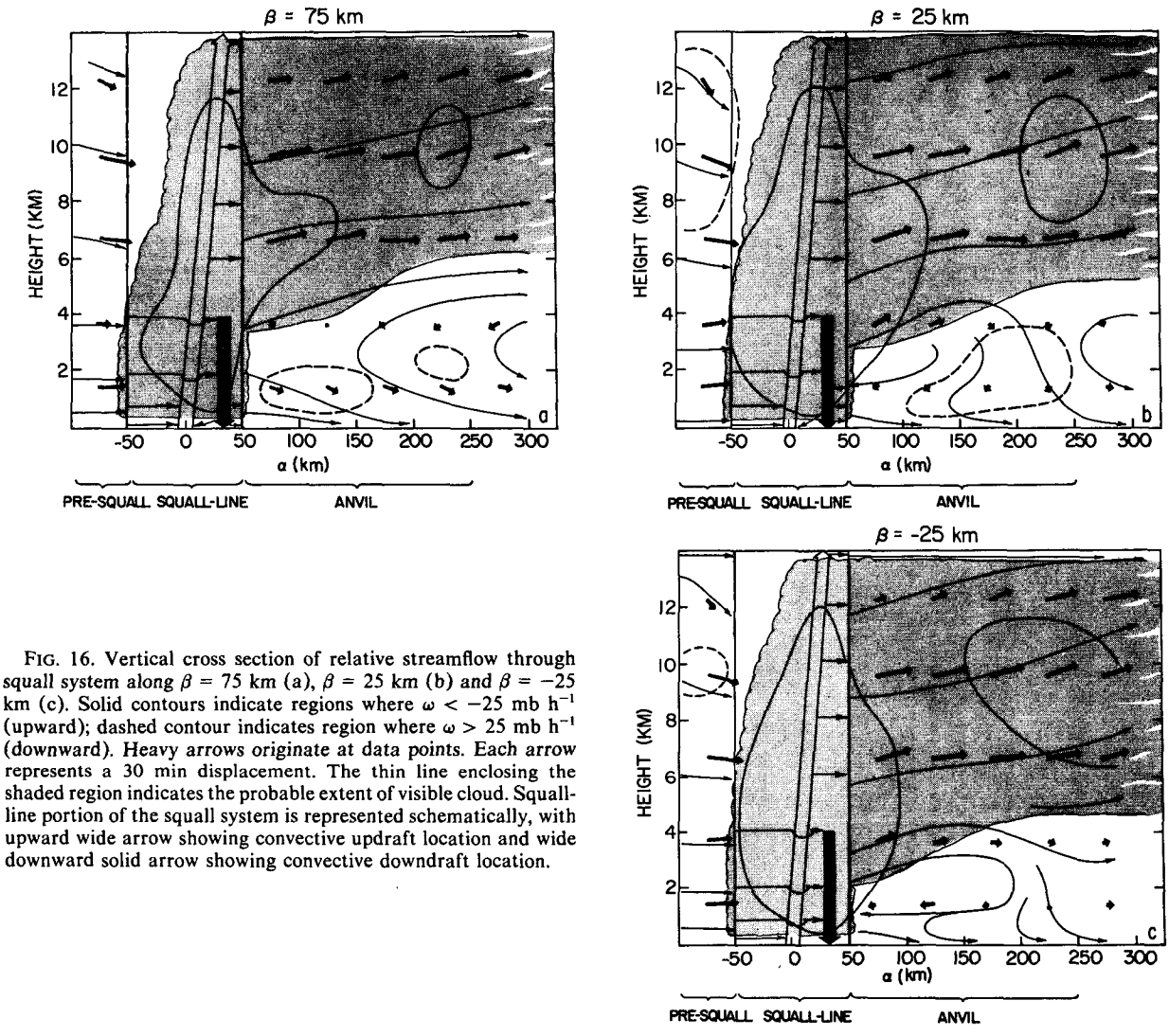

FIG. 16. Vertical cross section of relative streamflow through squall system along $\beta = 75$ km (a), $\beta = 25$ km (b) and $\beta = -25$ km (c). Solid contours indicate regions where $\omega < -25$ mb h^{-1} (upward); dashed contour indicates region where $\omega > 25$ mb h^{-1} (downward). Heavy arrows originate at data points. Each arrow represents a 30 min displacement. The thin line enclosing the shaded region indicates the probable extent of visible cloud. Squall-line portion of the squall system is represented schematically, with upward wide arrow showing convective updraft location and wide downward solid arrow showing convective downdraft location.

only. Updrafts and downdrafts in the squall-line region, shown schematically in Fig. 16, are based on the calculations in Section 6c and shown in Fig. 13. The cloud boundary included in Fig. 16 was drawn by enclosing regions of upward motion.

The streamflow in Fig. 16 strongly resembles the ideal flow in Fig. 1, especially the upward sloping streamlines in the anvil cloud, the downward sloping streamlines below the anvil base, and the near stagnation of the flow just below the base of the anvil. The streamlines in and below the anvil bear some resemblance to the updraft and downdraft streamlines of the propagating model of a traveling convective system described by Moncrieff and Miller (1976) and Moncrieff (1981). The squall-line region in Fig. 16 is characterized by inflow into convective updrafts and divergent outflow from convective downdrafts below 900 mb (~1 km). Between 900 and 650 mb, inflow from the front of the squall line feeds the convective downdrafts. Above 650 mb, the convective updrafts detrain into the anvil region.

The largest differences between the streamflow in Fig. 16 and the ideal flow in Fig. 1 involve the flows at 850 mb (1.5 km) and 650 mb (3.7 km). Figs. 16b and 16c show the 850 mb flow directed into the squall-line downdrafts from both the front and rear of the squall-line region, rather than from the front only. This result is expected from the 850 mb relative wind field seen in Fig. 6b. The 650 mb flow shown in Fig. 16c is outward from the rear of the squall system, but inward, as in Fig. 1, in Figs. 16a and 16b. These differences between the observed and ideal streamflow are not great and do not occur throughout the squall system. The average structure of the system is well represented by Fig. 1.

8. Conclusions

In past studies, air motions associated with tropical squall lines have been inferred from the thermodynamic properties of air flowing in and out of the storms (Hamilton and Archbold, 1945; Zipser, 1969,

1977; Obasi, 1974; Betts *et al.*, 1976; Houze, 1977), from numerical modeling (Brown 1979; Rosenthal, 1980), and from comparisons with mid-latitude squall lines (Sanders and Paine, 1975; Sanders and Emanuel, 1977; Ogura and Liou, 1980). These inferences have led to a qualitative model of the mesoscale flow associated with a tropical squall system (Fig. 1). In this paper, we have tested this model by compositing radar and wind observations in a moving coordinate system attached to a tropical squall line. The composite wind observations show the horizontal flow, divergence and vertical velocity on the mesoscale in the squall system and its nearby environment. The composite airflow is generally consistent with the qualitative model. Our analysis, however, extends the qualitative model by providing for the first time a quantitative field of vertical velocity for the squall system.

The composite radar data delineate the mean positions of the two basic components of the squall system: the convective squall-line region and the stratiform anvil region. Comparison of the composite airflow pattern and composite radar echo pattern shows fundamentally different mesoscale flow patterns associated with the squall-line and anvil regions. The squall-line region was characterized by boundary-layer convergence, which fed deep convective updrafts. The circulation in the anvil region, on the other hand, was characterized by mid-level convergence, which fed a mesoscale updraft within the anvil cloud and a mesoscale downdraft below the anvil. Any mesoscale divergence or vertical velocity pattern that is not decomposed into separate squall-line and anvil components will be a mixture of the basically different circulations in these two regions.

Prior to this study, knowledge of the mesoscale anvil circulation was qualitative, and in the case of the anvil updraft, speculative. Now there can be no question that the anvil updraft exists.

Further work should be done with the vertical and horizontal velocity fields derived for this squall system. The water vapor field and radar precipitation pattern can be used in conjunction with the wind field to study the water budget of the system. Clarification of the water budget will lead to more precise calculation of mass and heat transports by tropical convection (Houze *et al.*, 1980; Leary and Houze, 1980; Houze and Cheng, 1981). Vorticity may be computed from the composite wind field, and the momentum and vorticity budgets of the squall system may also be studied. Finally, since the squall system we have investigated is but one example, the composite flow patterns of other tropical squall systems should be derived and compared with the present case.

Acknowledgments. Dr. E. J. Zipser of NCAR has assisted the authors on this study in many ways. Both authors have been visitors with Dr. Zipser's GATE group at NCAR during the course of this study. Mr. M. D. Albright and Mr. E. E. Recker provided the authors with rawinsonde data in highly usable form. During the GATE Woods Hole Seminar in 1979, Prof. William Gray of Colorado State University strongly encouraged Prof. Houze to pursue the idea of compositing winds with respect to the GATE radar data. This research has been supported by the Global Atmospheric Research Program, Division of Atmospheric Sciences, National Science Foundation and the GATE Project Office, National Oceanic and Atmospheric Administration, under Grant ATM78-16859. This paper is Contribution No. 590, Department of Atmospheric Sciences, University of Washington.

REFERENCES

Arkell, R., and M. Hudlow, 1977: *GATE International Meteorological Radar Atlas.* Environmental Data Service, NOAA, [Govt. Printing Office (Stock No. 003-091-00038-1); NTIS PB-277 233/3G1], 222 pp.

Betts, A. K., R. W. Grover and M. W. Moncrieff, 1976: Structure and motion of tropical squall lines over Venezuela. *Quart. J. Roy. Meteor. Soc.*, **102,** 395–404.

Brown, J. M., 1979: Mesoscale unsaturated downdrafts driven by rainfall evaporation: A numerical study. *J. Atmos. Sci.*, **36,** 313–338.

Cheng, C.-P., 1981: Numerical simulation of the dynamics, cloud microphysics and radar echo structures of tropical and mid-latitude convection. Ph.D. dissertation, University of Washington, 217 pp.

——, and R. A. Houze, Jr., 1979: The distribution of convective and mesoscale precipitation in GATE radar echo patterns. *Mon. Wea. Rev.*, **107,** 1370–1381.

Fortune, M., 1980: Properties of African disturbance lines inferred from time-lapse satellite imagery. *Mon. Wea. Rev.*, **108,** 153–168.

Frank, W. M., 1978: The life cycles of GATE convective systems. *J. Atmos. Sci.*, **35,** 1256–1264.

Fritsch, J. M., 1975: Cumulus dynamics: Local compensating subsidence and its implication for cumulus parameterization. *Pure Appl. Geophys.*, **113,** 851–867.

——, and C. F. Chappell, 1980: Numerical prediction of convectively driven mesoscale pressure systems. Part II: Mesoscale model. *J. Atmos. Sci.*, **37,** 1734–1762.

——, and R. A. Maddox, 1981a: Convectively driven mesoscale weather systems aloft. Part I: Observations. *J. Appl. Meteor.*, **20,** 9–19.

——, and ——, 1981b: Convectively driven mesoscale weather systems aloft. Part II: Numerical simulations. *J. Appl. Meteor.*, **20,** 20–26.

Gaynor, J. E., and R. A. Mandics, 1978: Analysis of the tropical marine boundary layer during GATE using acoustic sounder data. *Mon. Wea. Rev.*, **106,** 223–232.

Haltiner, G. J., and Frank L. Martin, 1957: *Dynamical and Physical Meteorology.* McGraw-Hill, 470 pp.

Hamilton, R. A., and J. N. Archbold, 1945: Meteorology of Nigeria and adjacent territory. *Quart. J. Roy. Meteor. Soc.*, **71,** 231–262.

Houze, R. A., Jr., 1975: Squall lines observed in the vicinity of the *Researcher* during Phase III of GATE. *Preprints 16th Radar Meteor. Conf.*, Houston, Amer. Meteor. Soc., 206–209.

——, 1977: Structure and dynamics of a tropical squall-line system observed during GATE. *Mon. Wea. Rev.*, **105,** 1540–1567.

——, 1981: Structure of atmospheric precipitation systems—A global survey. *Radio Sci.*, **16,** 671–689.

——, and A. K. Betts, 1981: Convection in GATE. *Rev. Geophys. Space Phys.*, **19,** 541–576.

——, and C.-P. Cheng, 1977: Radar characteristics of tropical convection observed during GATE: Mean properties and trends over the summer season. *Mon. Wea. Rev.*, **105,** 964–980.

——, and ——, 1981: Inclusion of mesoscale updrafts and downdrafts in computations of vertical fluxes by ensembles of tropical clouds. *J. Atmos. Sci.*, **38,** 1751–1770.

——, ——, C. A. Leary and J. F. Gamache, 1980: Diagnosis of cloud mass and heat fluxes from radar and synoptic data. *J. Atmos. Sci.*, **37,** 754–773.

——, S. G. Geotis, F. D. Marks, Jr. and A. K. West, 1981: Winter monsoon convection in the vicinity of North Borneo, Part I: Structure and time variation of the clouds and precipitation. *Mon. Wea. Rev.*, **109,** 1595–1614.

Hoxit, T. R., C. F. Chappell and J. M. Fritsch, 1976: Formation of mesolows or pressure troughs in advance of cumulonimbus clouds. *Mon. Wea. Rev.*, **104,** 1419–1428.

Hudlow, M. D., 1979: Mean rainfall patterns for the three phases of GATE. *J. Appl. Meteor.*, **18,** 1656–1669.

——, V. Patterson, P. Pytlowany, F. Richards and S. Geotis, 1980: Calibration and intercomparison of the GATE C-band weather radars. NOAA Tech. Rep. EDIS 31, 98 pp. [Center for Environmental Assessment Services, NOAA, 3300 Whitehaven NW, Washington DC 20235].

Leary, C. A., 1978: Mesoscale organization in tropical cloud clusters. Ph.D. dissertation, University of Washington, 219 pp.

——, 1979: Behavior of the wind field in the vicinity of a cloud cluster in the Intertropical Convergence Zone. *J. Atmos. Sci.*, **36,** 631–639.

——, and R. A. Houze, Jr., 1979a: The structure and evolution of convection in a tropical cloud cluster. *J. Atmos. Sci.*, **36,** 437–457.

——, and ——, 1979b: Melting and evaporation of hydrometeors in precipitation from the anvil clouds of deep tropical convection. *J. Atmos. Sci.*, **36,** 669–679.

——, and ——, 1980: The contribution of mesoscale motion to the mass and heat fluxes of an intense tropical convection system. *J. Atmos. Sci.*, **37,** 784–796.

LeMone, M. A., and E. J. Zipser, 1980: Cumulonimbus vertical velocity events in GATE. Part I: Diameter, intensity and mass flux. *J. Atmos. Sci.*, **37,** 2444–2457.

Lilly, D. K., 1960: On the theory of disturbances in a conditionally unstable atmosphere. *Mon. Wea. Rev.*, **88,** 1–17.

Maddox, R. A., 1980: An objective technique for separating macroscale and mesoscale features in meteorological data. *Mon. Wea. Rev.*, **108,** 1108–1121.

Mandics, P. A., and F. F. Hall, Jr., 1976: Preliminary results from the GATE acoustic echo sounder. *Bull. Amer. Meteor. Soc.*, **57,** 1142–1147.

Mansfield, D. A., 1977: Squall-lines observed during GATE. *Quart. J. Roy. Meteor. Soc.*, **103,** 569–574.

Moncrieff, M. W., 1981: A theory of organized steady convection and its transport properties. *Quart. J. Roy. Meteor. Soc.*, **107,** 29–50.

——, and M. J. Miller, 1976: The dynamics and simulation of tropical squall lines. *Quart J. Roy. Meteor. Soc.*, **98,** 336–353.

Nitta, T., 1977: Response of cumulus updraft and downdraft A/B scale motion systems. *J. Atmos. Sci.*, **34,** 1163–1186.

Obasi, G. O. P., 1974: Some statistics concerning the disturbances lines of West Africa. *Preprints Symp. Tropical Meteorology,* Part II, Nairobi, Amer. Meteor. Soc., 52–66.

O'Brien, J. J., 1970: Alternative solutions to the classical vertical velocity problem. *J. Appl. Meteor.* **9,** 197–203.

Ogura, Y., and Y. L. Chen, 1977: A life history of an intense mesoscale convective storm in Oklahoma. *J. Atmos. Sci.*, **33,** 1458–1476.

——, and M. T. Liou, 1980: The structure of a mid-latitude squall line: A case study. *J. Atmos. Sci.*, **37,** 553–567.

——, Y.-L. Chen, J. Russell and S. T. Soong, 1979: On the formation of organized convective systems observed over the eastern Atlantic. *Mon. Wea. Rev.*, **107,** 426–441.

Reed, R. J., D. C. Norquist and E. E. Recker, 1977: The structure and properties of African wave disturbances during Phase III of GATE. *Mon. Wea. Rev.*, **105,** 369–387.

Riehl, H., and J. S. Malkus, 1958: On the heat balance in the equatorial trough zone. *Geophysica,* **6,** 503–538.

——, and J. Simpson, 1979: The heat balance of the equatorial trough zone, revisited. *Beitr. Phys. Atmos.*, **52,** 287–305.

Rosenthal, S. L., 1980: Numerical simulation of tropical cyclone development with latent heat release by the resolvable scales, II: Propagating small-scale features observed in the pre-hurricane phase. NOAA Tech. Rep. ERL 413-AOML 29, Research Laboratories, Boulder, 43 pp. [Government Printing Office].

Sanders, F., and K. A. Emanuel, 1977: The momentum budget and temporal evolution of a mesoscale convective system. *J. Atmos. Sci.*, **34,** 322–330.

——, and R. J. Paine, 1975: The structure and thermodynamics of an intense mesoscale storm in Oklahoma. *J. Atmos. Sci.*, **32,** 1563–1579.

Shupiatsky, A. B., G. N. Evseonok and A. I. Korotov, 1976: Investigation of clouds in the ITCZ with satellite and ship radar. *TROPEX-74,* Vol. 1, *Atmosphere,* Gidrometeorizdat, Leningrad, 515–520 (in Russian).

Suchman, D., and D. W. Martin, 1976: Wind sets from SMS images: An assessment of quality for GATE. *J. Appl. Meteor.*, **15,** 1265–1278.

Tourre, Y. M., 1979: The squall-line over West Africa and tropical eastern Atlantic Ocean during GATE. Ph.D. dissertation, University of Virginia, 122 pp.

Wilhelmson, R., 1974: The life cycle of a thunderstorm in three dimensions. *J. Atmos. Sci.*, **31,** 1629–1651.

Zipser, E. J., 1969: The role of organized unsaturated convective downdrafts in the structure and rapid decay of an equatorial disturbance. *J. Appl. Meteor.*, **8,** 799–814.

——, 1977: Mesoscale and convective-scale downdrafts as distinct components of squall-line circulation. *Mon. Wea. Rev.*, **105,** 1568–1569.